Separation and Purification Technology
Volume 240, 1 June 2020, 116630

NaA zeolite-coated meshes with tunable hydrophilicity for oil-water separation

Ghader Mahmodi [a], Shailesh Dangwal [a], Payam Zarrintaj [a], Mengfan Zhu [b], Yu Mao [b], David N. McIlroy [c], Mohammad Reza Saeb [d], Vahid Vatanpour [e], Joshua D. Ramsey [a], Seok-Jhin Kim [a]

Show more

https://doi.org/10.1016/j.seppur.2020.116630

Highlights

- Hydrophilicity of NaA mesh was controlled by using Si/Al ratio in zeolite crystal.
- The NaA meshes were regenerated by re-calcination, while keeping oil rejection rate more than 99%.
- The NaA zeolite mesh exhibited good stability in acidic, basic, and hot solution.

Abstract

NaA zeolite was fabricated on a stainless steel mesh by secondary growth method through optimizing aluminum/silicon ratio (ASR) to effectively separate oily water. The NaA zeolite-coated mesh with the highest superoleophobic property had an ASR of 1.21 and an oil contact angle of 163.7°. The highest membrane flux obtained was 13,513 L m^{-2} h^{-1} for an ASR = 0.91 and the highest separation efficiency was 99.5% for an ASR = 1.21. NaA zeolite meshes were recycled and reused for 15 cycles by rinsing the membrane with DI water between each test. The oil rejection rate of the mesh for ASR = 0 decreased approximately 2.7% after 4 cycles of separation, but the oil rejection rate of the meshes for ASRs = 0.3–182 did not change with 4 cycles of oil water separation, which is attributed to the uniformity of the NaA zeolite coating and its thermal stability. For long-term usage, the NaA zeolite meshes were regenerated by re-calcination, with an average oil rejection rate after three cyclic calcinations of more than 99.3%. In hot and corrosive solutions, the NaA zeolite meshes were stable, showing oil rejection rates above 99.3%. NaA zeolite meshes were also used for separation of various oils, such as n-hexane, mineral oil, olive oil, and diesel. The oil rejection rates were higher than 98.3% in all cases, which demonstrates that NaA zeolite mesh is very promising technology for oil/water separation applications.

Keywords

Zeolite; Membrane; Mesh; Hydrophilicity; Oil-water separation

1. Introduction

The availability of clean water has been an important issue around the globe, where the safety and maintenance of clean water sources is critical to environmental, societal and human health. Oil spills attract the attention of the public because of their negative impact on human health, the environment and regional economics [1], [2], [3]. Oil spills cause drastic human health issues such as vegetative-nervous symptoms, skin and mucous irritations, and also psychological effects. Moreover, deleterious effect of oil spills on diverse flora and fauna species is well known [4]. For instance, oil spillage from the tanker Tasman Spirit contaminated the environment, which affected the people health. The results indicated that the lymphocyte and eosinophil level in the blood of the people who work in neighboring the spoiling area was increased [5]. Consequently, the development of oil/water separation technology is a worldwide goal and challenge. Various methods for oil/water separation have been proposed to refine the water, such as coagulation, adsorption, air flotation, and sorption process [6], [7], [8], [9], [10], [11], [12]. However, these methods have drawbacks, such as high cost, large machinery and low efficacy [13], [14]. Membrane filters have been widely used in oil-water mixture treatment due to their high separation capability and facile operation conditions [15], [16]. Micro/nano and ultra-filtration membranes have also been utilized for oil-water separation [17], [18]. Typically, porous membranes, regardless of their construction, suffer from fouling, which reduces the permeation efficiency [13], [14], [17], [18]. For instance, polymeric membranes are attractive due to their effective selectivity, affordable cost, easy handling and low energy consumption [17], but are prone to fouling by natural organics, proteins and biofilms and corresponding decreases in flux over time. To remove foulants on the membrane surface, chemical rinsing is a proposed remedy, but strong oxidants can damage the membrane structure and decrease its lifetime. Moreover, high waste output is another underlying flaw associated with chemical rinsing which not only contaminate the environment, also threaten people health [19]. Thus, regardless of its own costs and benefits, efforts on the use of organic membranes have remained an open challenge to be resolved.

Inorganic membranes exhibit great potential for oil-water separation due to their proper chemical and physical properties, high durability and reusability [15]. Inorganic membranes are categorized as ceramic membranes and carbon-based membranes. Ceramic membranes are made from metal oxides (e.g. alumina, silica and zirconia), zeolite as well as metal organic framework [20]. Carbon-based membranes are formed from carbon nanotubes (CNT) and graphene [20]. Generally, ceramic membranes have attracted significant attention because of their excellent properties such as fouling resistance, and thermal and chemical stability [21], [22], [23]. Moreover, ceramic membranes are mechanically strong and durable to preserve performance for a long time and they can cope with high pressures in industrial applications [24]. However, ceramic membranes have some drawbacks such as low permanence, physical fragility, and also low salt rejection for practical seawater desalination [25]. Carbon-based membranes like carbon nanotubes have some benefits such as high surface area, antimicrobial activity, tunable pore size, surface chemistry and electrical conductivity [20]. In addition to being highly permeable and selective, graphene membranes provide uniform pore size distribution in membranes [7], [26]. Likewise, carbon-type membranes like ceramic membrane are thermally and chemically stable. However, carbon-based membranes show low resistance to fouling, and controlling the pore size distribution of the carbon-based membranes is difficult [27].

For treating oily wastewater, inorganic membranes, such as carbon nanotubes, graphene, and zeolite-based membranes have been proposed [28], [29], [30]. Zeolite membranes have attracted significant attention due to their high surface area, unique molecular sieving properties, and various pore sizes [31], [32]. Zeolites consist of aluminum, oxygen, and silicone with tetrahedral crystalline framework, which produces discrete pore sizes [33]. In particular, NaA zeolites have been used in membrane applications because of their unique properties, such as high thermal stability and tunable pore diameters from 0.3 to 0.5 nm using ion exchange of aquatic calcium or potassium salt [34], [35]. Kiadehi et al. synthesized a NaY zeolite using the secondary growth method on stainless-steel mesh for hydrogen separation. They reported that the NaY zeolite mesh improved the hydrogen permeation flux by approximately 12 times relative to a palladium composite membrane [36]. Jiang et al. synthesized hollow fiber CHA zeolite membranes with varied Si/Al ratios. CHA zeolite membranes with Si/Al ratios>2.9 showed the highest separation factor (>10,000), as compared to 5,000 for a Si/Al ratio of 2.7. They reported it is probably because the low Si/Al ratio resulted in low crystallinity of membranes and the incomplete crystallization or dissolution of CHA zeolite crystals. The optimized Si/Al ratio enhanced the membrane's stability in harsh environmental conditions, such as acidic

because the high crystalline zeolites were not blocked, unlike the lower Si/Al ratio membranes [37]. For alcohol/water separation, Li et al. improved stability of NaA zeolite membranes by adding a polyelectrolyte on the membrane surface, which produced a permeability of 875 g m^{-2} h^{-1} and ethanol separation of 99.8% [38]. Liu et al. investigated the effect of seeding methods, such as dip-coating, rubbing, and combinations of both rubbing and dip-coating, on the NaA zeolite membrane's performance. The combination of rubbing and dip-coating showed a more uniform seed layer and improved its performance for ethanol/water separation, as compared to separating dip-coating and rubbing seeding methods [39].

One of the major problems in commercial membrane is fouling phenomena, which cause to reduce the membrane permeability and performance. Fouling has a great effect on membrane efficiency which significant efforts have been made to decrease the membrane fouling [40], [41], [42], [43]. It was reported that the pristine polysulfone (PSF) ultrafiltration membranes performance was reduced because of the fouling phenomenon. In this regards, Ju et al. [40] synthesized the anti-fouling poly (ethylene glycol) diacrylate (PEGDA) membrane for oil/water separation. This membrane showed higher permeation and lower oil fouling than uncoated polysulfone (PSF) ultrafiltration membranes. Hydrophilic membrane surface absorbs water and prevent the fouling which is the one attractive approach is to develop anti-fouling membranes. Hydrophobic membranes are intrinsically vulnerable to oil fouling since hydrophobic materials are prone to adsorbing to the membrane surface due to their oleophilic properties [44], [45]. Using hydrophilic-material-coated meshes for oil/water separation is promising because they repel oil droplets and facilitate the removal of oil foulants. Materials such as hydrogel [46], ZnO [47], [48], [49], and TiO_2 [16], [50] have been coated on meshes to enhance hydrophilicity for oil/water separation. In spite of the aforementioned membranes' high oil rejection efficiencies, their structures are not compatible in hot, acidic, and basic solutions [51], [52]. Zeolite membranes are favorable because of their chemical, mechanical, thermally stable, and corrosion resistant properties. As shown in Table 1, in our previous studies [23], [53], boron and aluminum substituted MFI zeolite-coated meshes were developed for oil/water separation. The zeolite-coated meshes showed high oil rejection efficiency and high stability in acidic, basic, and hot solutions. The tetrahedral structure of the MFI zeolite provides a unique opportunity for functionalization with hydroxyl groups. However, there is a need for precisely tunable hydrophilicity as well as high separation efficiency involved in more zeolite structures for oily water treatment.

Table 1. Various inorganic hydrophilic materials coated on stainless steel mesh for hexane/water separation.

Inorganic materials	Flux (L $m^{-2}h^{-1}$)	Oil rejection rate (%)	Reference
PVP/TiO_2	16,500	~99%	16
Chitosan	21,535	>99%	43
Polyacrylamide	–	>99%	45
Hydrogel	–	>99%	46
ZnO	–	>95%	47
ZnO	–	>98%	49
MFI-type Zeolite	>80,000	>99%	23
Boron substituted MFI-type Zeolite	>14,000	>99%	53
SiO_2	26,280	>99%	51

In this work, a NaA zeolite-coated membrane with tunable hydrophilicity was prepared using a secondary growth method and placed in practice for high-level oil/water separation. The zeolite-based membrane was calcinated and retested to evaluate the oil/water separation efficiency, reusability, regenerability, and stability. The ratio of Al/Si (ASR) in the NaA zeolite mesh was considered as a key factor. Moreover, the NaA zeolite-coated mesh was tested for various oils including olive oil, mineral oil, and diesel to assess the effect of the type of oil on oil/water separation efficacy. The degree of hydrophilicity was evaluated along with for mesh stability analysis in in acidic, basic and hot solutions. Such modification paves a way to produce a cost-effective and high efficient membrane to effectively treat oily wastewater such as produced water.

2. Material and methods

2.1. NaA seed synthesis

The procedure for preparing NaA seeds has been previously reported by Zhang et al. [54] and only an abbreviated description is provided here. Sodium aluminate (Al (Al_2O_3):50–56%, Na (Na_2O):40–45%), sodium metasilicate nonahydrate (≥98% purity) and sodium hydroxide (99.99%) were purchased from Sigma-Aldrich (USA). Sodium aluminate (7.16 g) was added to 35 g of deionized (DI) water, and the resulting aluminate solution was stirred for 5 min. Silicate solution was produced by adding 20.72 g of sodium metasilicate nonahydrate to 42 g of DI water, and the resulting solution was stirred at 50 °C for 10 min. Subsequently, the silicate solution was gradually added to the aluminate solution under vigorous stirring for 15 min. The resulting solution was transferred into a hydrothermal vessel and processed at 100 °C for 4 h. The synthesized NaA zeolite powder was washed in deionized water in a centrifuge and dried. Then, NaA seeding solution (3 wt%) was obtained by adding 1.5 g of NaA zeolite powder into 50 mL of DI water. The pristine stainless steel mesh (0.9 in × 0.9 in) was washed and cleaned by ethanol, acetone, and deionized water, in that order. The cleaned mesh was dried overnight at 50 °C in an oven. Before hydrothermal synthesis, the cleaned mesh was seeded by dip-coating method (immersed in in NaA seeding solution) for 5 min (Fig. 1a).

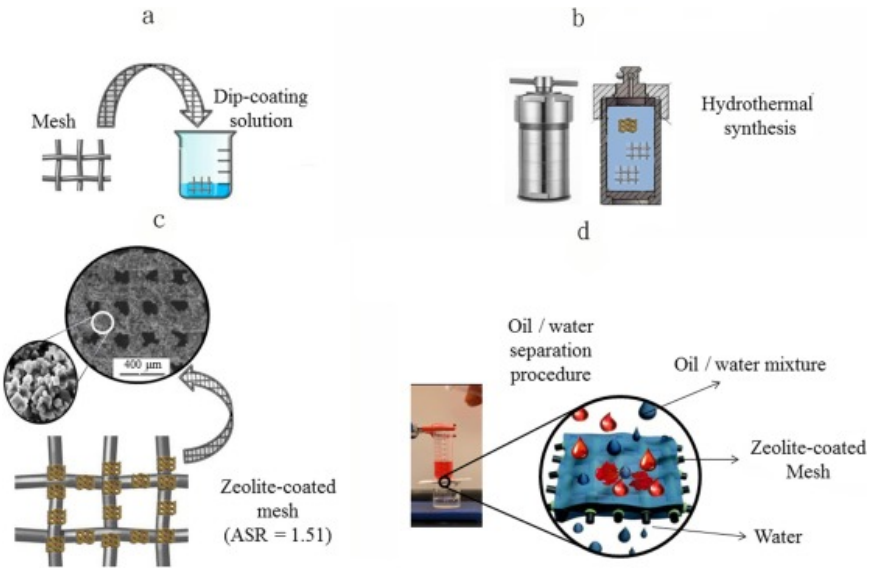

Download : Download high-res image (234KB)

Download : Download full-size image

Fig. 1. Schematic illustration of the synthetization of the NaA zeolite coated mesh (a) dip-coating, (b) hydrothermal synthesis, (c) zeolite-coated mesh, and (d) oil/water separation procedure.

2.2. Zeolite-coated mesh synthesis

The synthesis solution for secondary growth was prepared using the following procedure [54]: Sodium hydroxide was dissolved in DI water under vigorous stirring for 5 min. Then, sodium aluminate was added and the resulting solution was stirred for 3 h. Subsequently, a uniform solution was obtained by adding sodium metasilicate nonohydrate and the solution was stirred vigorously for 30 min. The molar ratio of the solution was maintained at $H_{18}Na_2O_{12}Si$: NaOH: H_2O:$NaAlO_2$ = 1:1.89:172:X, respectively. The value of X was varied from 0 to 1.82. The dried seeded mesh was kept vertically inside a 20 mL autoclave reactor which contained 18 mL of synthesis solution and hydrothermal synthesis was carried out at 100 °C for 4 h (Fig. 1b and c). After hydrothermal growth, the fabricated membrane was taken out from the reactor and washed with DI water. Then, the NaA zeolite coated mesh was calcined at 450 °C for 4 h with a heating and cooling rate of 30 °C/h.

2.3. Oil/Water separation experiments

To evaluate the NaA zeolite meshes performance for oil/water separation, it was placed between two Teflon sheets and sealed completely by epoxy resin, as reported in our previous studies [23], [53]. The oil/water separation efficiency was r

different oils, such as n-hexane, diesel fuel, olive oil, and mineral oil. To investigate the fouling resistance and endurance of the NaA zeolite coated meshes, oil/water separation was conducted for 15 separation cycles. The oil was colored with Sudan Red 4 (Amresco company, USA) to distinguish it from water. 20 mL of DI water was poured on top of the fabricated membranes before the test for pre-wetting. The oil/water mixture (50% v/v, 40 mL) was poured on the surface of the zeolite meshes (with 6.36 cm^2 surface area) and the separation was driven by gravity (Fig. 1d). After few seconds (9–15 s depends on ASR), water permeated the mesh while the oil was repelled beyond the mesh surface (Video S1 in normal water condition and Video S2 in hot water solution). The oil rejection rate is defined and evaluated as follows:

$$\eta = 1 - \frac{C_i}{C_0} \tag{1}$$

where η stands for oil rejection rate, and C_0 and C_i are the concentration of oil in feed and permeate, respectively. The permeation flux was calculated using the following equation:

$$J = \frac{V}{A \times t} \tag{2}$$

where J is permeation flux (L m^{-2} s^{-1}), V (L) is the volume of the permeate, A (m^2) is the effective membrane surface area, and t (s) is the permeation time.

2.4. Characterization

A FEI Quanta 600F field emission scanning electron microscope (SEM) equipped with an Energy Dispersive Spectrometry (EDS) X-ray microanalysis unit was used to examine the surface morphology and elemental dispersion of the NaA zeolite mesh, respectively. The phase and crystal structure of the NaA zeolite mesh was characterized by X-ray powder diffraction (XRD) (Bruker D8-A25-ADVANCE) scanning from 2Θ of 5–40°. UV–vis spectrophotometer (Beckman Coulter DU 730) and the analytical weighing scale (Cole-Parmer Instrument Company-USA) was used to measure the oil concentration in the permeate. A contact angle goniometer (Rame-Hart Goniometer model 250) was used to measure the contact angles of the mesh at room temperature. While measuring contact angle, a section of the mesh was put on plastic coverslips to hold the mesh and to avoid its submersion into water. To obtain a reliable oil contact angle (OCA), the results reported herein are on the average of three measurements on the three different areas of the NaA zeolite mesh. Moreover, n-hexane (2 μL) was descended on the membrane surface for each contact angle measurement.

3. Results and discussion

3.1. Characterization of NaA zeolite mesh

The surface morphologies of the pristine and NaA zeolite coated meshes were examined by SEM. Fig. S1 shows the SEM images of pristine mesh with average pore size of ~150 μm diameter, where the inset shows that the bare mesh has a smooth surface [51]. For an ASR = 0 (Fig. 2a0–a2), the coating is highly nonuniform when compared with those processed with a higher ASR (0.3–1.82), which indicates the crystallization was incomplete. However, with increasing ASR (Fig. 2b–e), it was found that the mesh surface was entirely coated by NaA zeolite crystals. The pore size of the meshes decreased from 150 μm (pristine mesh, Fig. S1) to about 10 μm (ASR = 1.21, Fig. 2e0). As shown in Fig. 2c2, d2, and e2, the NaA zeolite meshes were aggregated on the stainless steel mesh surface and showed higher surface roughness, a very crucial factor for the underwater super-oleophobicity of the mesh [51], [55]. For ASR > 1.21 (Fig. S1b and S1c), the mesh pores were found to be partially or completely blocked, which drastically reduced water flux.

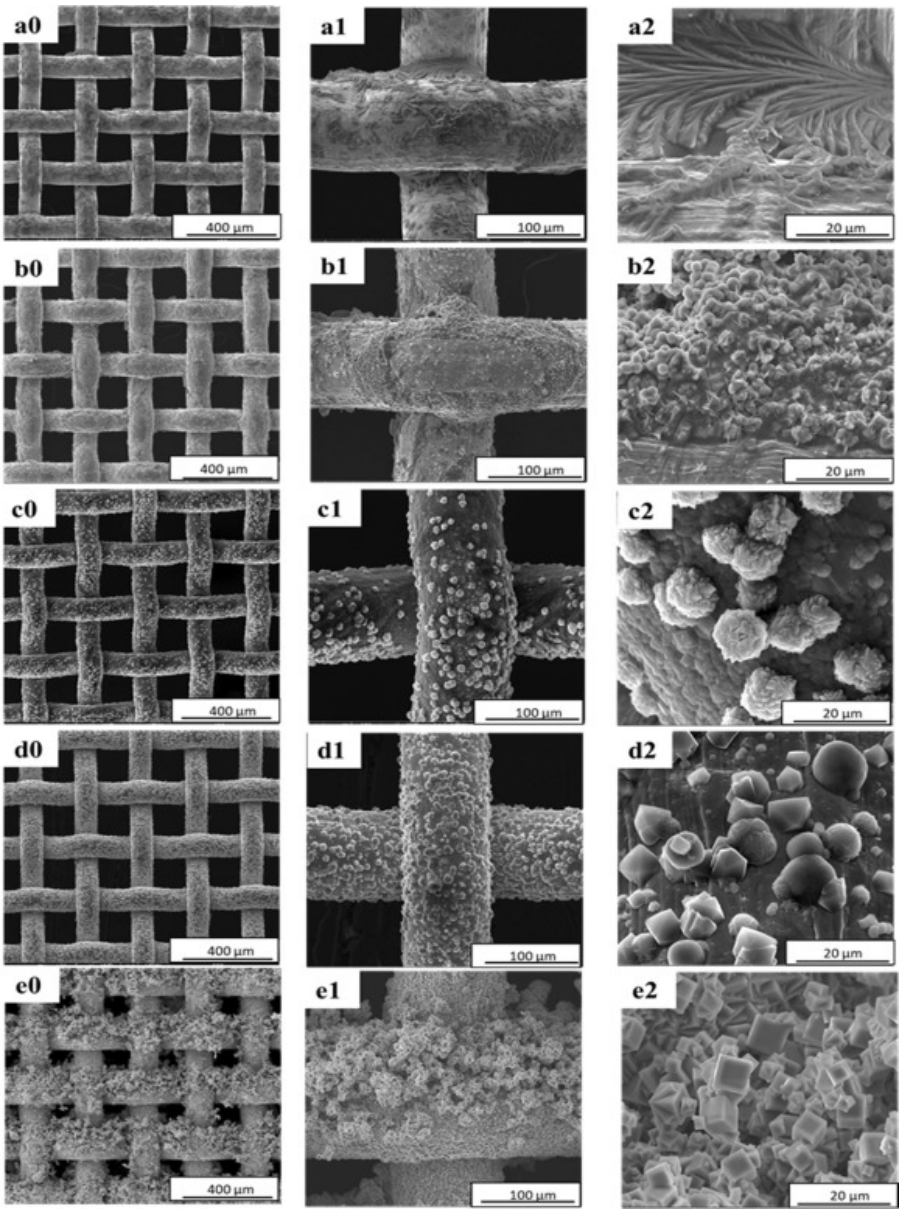

Download : Download high-res image (1MB) Download : Download full-size image

Fig. 2. SEM photos of NaA zeolite coated mesh with (a) ASR=0, (b) ASR=0.31, (c) ASR=0.61, (d) ASR=0.91, and (e) ASR=1.21.

To evaluate the stoichiometry of the NaA zeolite mesh, EDS was performed on the pristine and the zeolite coated mesh (ASR=1.21). Based on Fig. S2a, iron, chromium, and nickel are the main components of the pristine mesh, as expected per the manufacturer's specifications. The carbon peak is attributed to the carbon adhesive used to hold the mesh onto the SEM specimen holder. For the zeolite coated mesh with ASR=1.21 (Fig. S2b), the elemental stoichiometry is 49% O, 15% Na, 15% Al, and 12% Si, which confirms that NaA zeolite film has been deposited on the stainless steel mesh.

The XRD pattern of NaA zeolite powder, pristine stainless steel mesh, and NaA zeolite mesh are shown in Fig. S3. The XRD pattern of the NaA zeolite powder (Fig. S3c) ranges from 5 to 35°, which corresponds to the characteristic peaks of NaA zeolite crystals [56], [57]. The XRD pattern of NaA zeolite coated mesh (Fig. S3a) presents characteristic peaks of NaA zeolite crystals, as well as some peaks coming from the stainless steel mesh [36], [56], [57], which is to be expected.

3.2. Wettability study of NaA zeolite coated mesh

The wettability of pristine mesh and NaA zeolite coated mesh were assessed by water contact angle (WCA) and oil contact angle (OCA) measurements. As shown in Fig. S4a, for a 2 μL DI water dropped on the surface of the pristine mesh, the WCA is 115.3°, indicative of the intrinsic hydrophobicity of the pristine mesh. For the zeolite coated mesh (ASR=1.21), the WCA is 0° (Fig. S4b), indicating that the NaA zeolite significantly increases the hydrophilicity of the mesh. To study the effect of ASR on the wettability of membrane, underwater OCA was measured using n-hexane (2 μL). Fig. 3 shows the underwater super-oleophobic property of zeolite meshes for various ASRs. The underwater OCA of the zeolite mesh (ASR=1.21) is 163.7° (Fig. S5c), indicating that the underwater super-oleophobicity of the membrane increases with the introduction of aluminum. In other words, the oil-fouling of the zeolite meshes decreases with increasing ASR from 0 to 1.21.

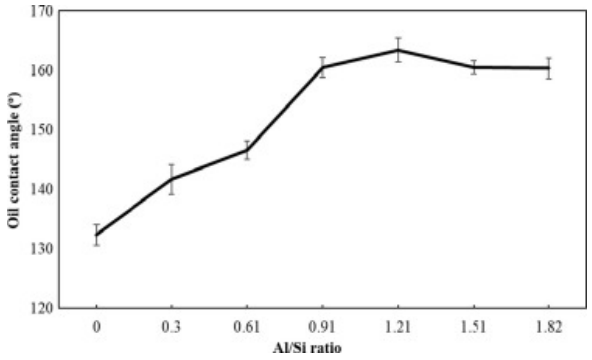

Download : Download high-res image (55KB) Download : Download full-size image

Fig. 3. Underwater oil contact angles of n-hexane on the zeolite-coated mesh as a function of Al/Si ratio.

With increasing ASR from 0 to 1.21, OCA value increase from 132.0° to 163.7° (Fig. 3) and then slightly decreases to 160.7° for an ASR=1.82. Given the high levels of OCA (e.g., 163.7° at ASR=1.21), it is possible that a water layer forms between the NaA zeolite coated mesh and the n-hexane droplet [23], [55], [58]. If NaA zeolite crystals are engaged and anchor the water layer, it could repel the oil from adhering to the surface [23], [53]. The empty 2p orbitals of Al^{3+} ions have an enormous tendency to link with water, resulting in an increase in the density of hydroxyl groups on the surface of the NaA zeolite crystals. Therefore, the enhanced hydrophilicity of the hydroxylated surface remarkably helps to reject oil molecules [23], [53]. Assuming that the capacity of empty 2p orbitals of Al^{3+} ions is limited, after incrementing the ASR there was not considerable increase in OCA values. However, the OCA decreased slightly for ASR>1.21.

3.3. Zeolite-coated mesh performance for oil/water separation

As shown in Fig. 4, the oil rejection rate for ASR=0 decreased from 96.2% to 93.7% after 4 separation cycles, probably because there are no Al^{3+} ions that can enhance membrane surface hydrophilicity. However, the oil rejection rates of the mesh with ASRs of 0.3–1.82 were higher than that of ASR=0, and the mesh with ASR of 1.21 showed the highest oil rejection rate of 99.4% during 4 separation cycles. Since Al^{3+} ions were incorporated in the zeolite structure by replacing Si^{4+} ions, the empty 3p orbital on the Al^{3+} ion accept unaccompanied pair electrons from electron donors. Therefore, it is expected that a larger concentration of Al^{3+} ions will increase the oil rejection [34], [23]. In other words, the higher the concentration of Al^{3+} ions incorporated into the membrane structure, the higher the oil separation rate. Once an oil/water mixture liquid is applied to the membrane surface, hydroxyl groups attach to Al^{3+} ions through synchronized bonds [37], [23], which converts the surface of the mesh from hydrophobic to hydrophilic through hydrogen bonding of hydroxyl groups. Consequently, a larger ASR in the mesh increases the connection between water and the mesh surface and leads to a higher oil rejection rate [23], [54].

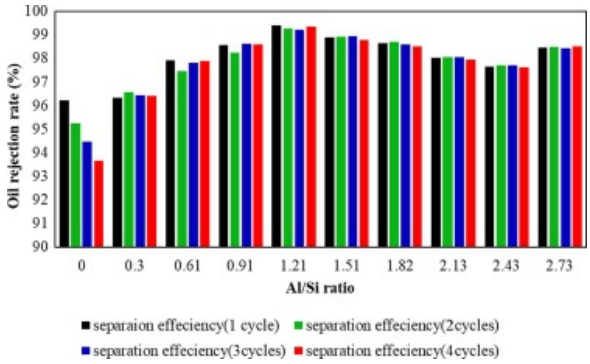

Download : Download high-res image (172KB) Download : Download full-size image

Fig. 4. The oil rejection rate of NaA zeolite-coated mesh as a function of Al/Si ratio.

Fig. 5 is a plot of the permeation performance of NaA zeolite-coated meshes as a function of ASR. According to Fig. 5, the water flux increases with increasing ASR, where the maximum water flux of 13,356 L m^{-2} h^{-1} is achieved for an ASR = 0.91 and subsequently decreases with increasing ASR. This decreasing trend of the flux for ASR > 0.91 is attributed to the combination of underwater OCA and the decreasing pore size of the zeolite coated mesh (Figs. 2 and S2) [16]. Since the underwater OCA value is proportional to water penetration across the mesh [16], [59], the smaller OCA could decrease water penetration across the zeolite mesh, indicative of a weakening of the water capillary films. To further evaluate oil separation potential of the NaA zeolite coated mesh, the best zeolite mesh (ASR = 1.21) was selected and tested in various oils, such as n-hexane, mineral oil, olive oil, and diesel fuel. Fig. 6 shows that the oil rejection rates for various oils were above 98.1%.

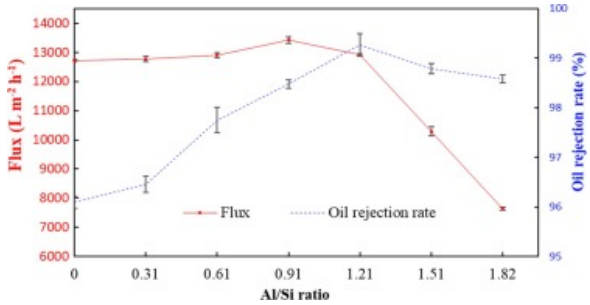

Download : Download high-res image (87KB) Download : Download full-size image

Fig. 5. Effects of varied Al/Si ratios on water flux and oil rejection rate of the zeolite-coated meshes.

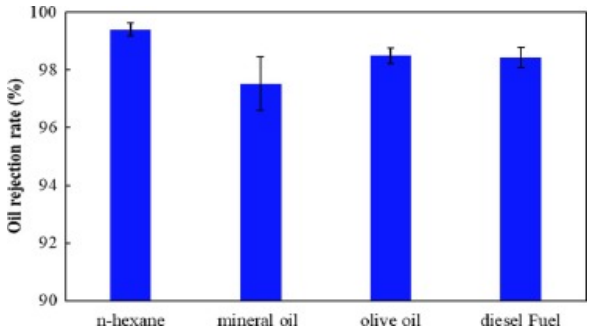

Download : Download high-res image (63KB) Download : Download full-size image

FEEDBACK

Fig. 6. Oil rejection rate of NaA zeolite-coated mesh with ASR=1.21 for various oils.

3.4. Reusability and stability of the NaA zeolite coated mesh membrane for oil water separation

One of the primary challenges in membrane technology is fabricating anti-fouling membrane for long-term usage. Generally, membranes are highly prone to fouling, which reduces their separation efficiency and increases energy consumption [60]. To test the long-term reusability of the zeolite mesh for oil/water separation, we selected the mesh with ASR=1.21 and evaluated for multiple separation cycles. After washing the used membrane with DI water and waiting for 10 min, the next oil/water separation was performed. As shown in Fig. 7, the oil rejection rate for the zeolite mesh with ASR=1.21 after operating for 15 separation cycles remains more than 99%.

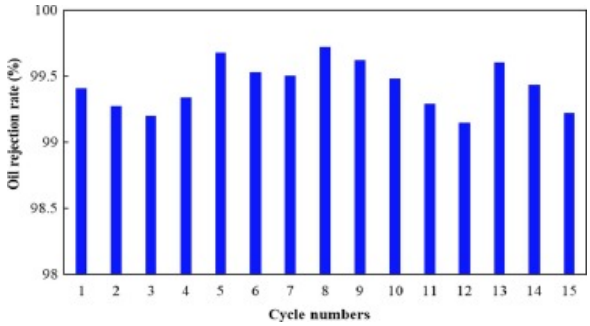

Download : Download high-res image (91KB) Download : Download full-size image

Fig. 7. Oil rejection rate of the NaA zeolite-coated (ASR=1.21) mesh during 15 separation cycles of oil/water mixture.

The results indicated impressive stability and reusability of the zeolite mesh. To assess the stability, the zeolite mesh was tested in acidic, basic, and hot oil/water mixtures, respectively. Before the test, the mesh was pre-wetted by 1 M HCl (acidic), 1 M NaCl, and hot water, respectively.

Fig. 8 shows that the zeolite mesh is quite stable in corrosive or hot aqueous solutions. The average oil rejection rate in normal (23 °C), hot water (90 °C), acidic, and basic solutions is 99.4%, 99.7%, 99.4%, and 99.4%, respectively. The zeolite coated meshes have high stability in corrosive or hot aqueous solutions, which makes them potential candidates for industrial oil/water separation applications. SEM images of the mesh before and after testing in corrosive or hot aqueous solutions are presented in Fig. 9 to show the mechanical stability of the zeolite layer. Although some cracks are observed on the mesh surface, the NaA zeolite structure remains unchanged, indicative of the high stability of the NaA zeolite structure in harsh conditions, which is supported by permeation results.

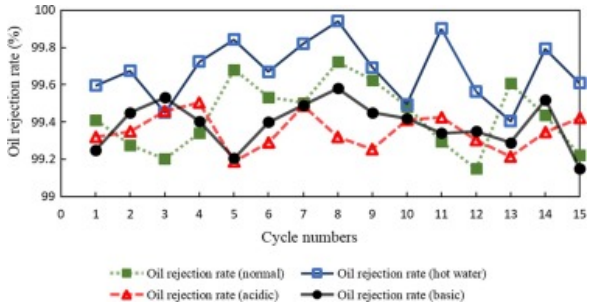

Download : Download high-res image (128KB) Download : Download full-size image

Fig. 8. Oil/water separation rate of NaA zeolite-coated mesh with ASR=1.21 in ordinary, acidic, basic, and hot sol

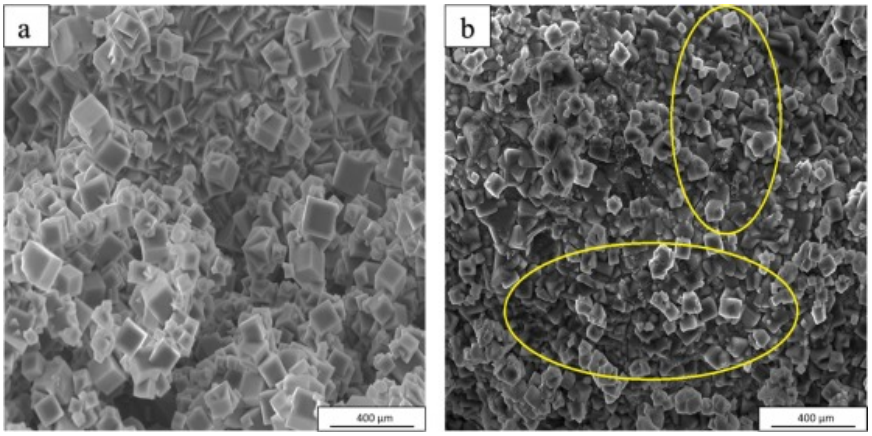

Download : Download high-res image (427KB) Download : Download full-size image

Fig. 9. SEM photos of NaA zeolite-coated mesh a) before and b) after oil/water separation test in harsh environmental conditions.

Moreover, reusability is one of the most significant features of the zeolite mesh. We examined the reusability by the re-calcination process. The used zeolite coated-mesh were re-calcined in the oven at 550 °C for 6 h with heating and cooling ramping rates of 30 °C/h. During the calcination process, the organic material (epoxy, rubber rings, and adhered oils) attached to the mesh were burned away. Upon subsequent use, the oil rejection rate is nearly unchanged and the average oil rejection rate after 3 re-calcination cycles is > 99.4% (Fig. 10), as compared to that before calcination (99.7%). After 4 cycles of calcination, the zeolite-coated mesh exhibit reproducibility in terms of oil/water separation performance, which demonstrates that the recalcination is a simple and fast method to refresh the used mesh without sacrificing performance. The re-calcination can not only save the membrane regeneration time, but also decreases the operational cost [23].

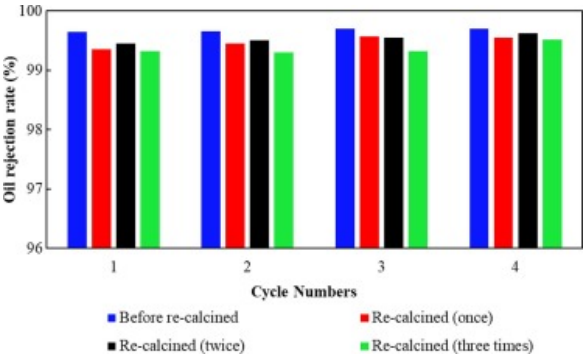

Download : Download high-res image (106KB) Download : Download full-size image

Fig. 10. Oil rejection rate of the NaA zeolite-coated meshes with ASR = 1.21 before and after calcination for oil/water separation.

To further investigate the stability of the zeolite mesh, EDS has been performed before and after cyclic re-calcinations to observe changes in the zeolite stoichiometry and is summarized in Table 2. The ASR decreases slightly from 1.21 to 1.11 after 3 re-calcination cycles, which is attributed to the loss of Al. During the re-calcination process, organic components, epoxy, and residual oil on the mesh surface can be burned and converted to form water [61]. The re-calcination process in the presence of water under 550 °C causes dealumination in the zeolite structure.

Table 2. Elemental surface composition of NaA zeolite coated mesh (ASR=1.21) before and after 3 times re-calcination.

Samples	EDS atomic %		Al/Si
	Al	Si	
Before re-calcination	21.59	17.86	1.21[a]
After 1st re-calcination	21.10	17.52	1.20[b]
After 2nd re-calcination	20.55	17.24	1.19[b]
After 3rd re-calcination	16.61	14.98	1.11[b]

a Before separation test.

b After separation test.

4. Conclusion

We synthesized NaA-type zeolite-coated mesh and controlled hydrophilicity by varying the Al/Si ratio (ASR). The zeolite mesh with ASR=1.21 showed the highest separation efficiency of 99.5%. By increasing ASR from 0 to 1.21, the oil contact angle increased from 132° to 163.7°, an indication of increasing hydrophilicity of the mesh. However, with further increasing of the ASR from 1.21 to 1.82, the oil contact angle slightly decreased to 160°. NaA zeolite layer formation on the mesh was confirmed by EDS, with a composition of 49% O, 15% Na, 15% Al, and 12% Si, respectively. The zeolite-coated mesh (ASR=0.91) had a water flux of >13,513 L m^{-2} h^{-1} and the zeolite-coated mesh (ASR=1.21) had an oil rejection rate of >99.4%. The zeolite mesh exhibited good stability, reproducibility, and refreshability in corrosive or hot aqueous solutions. The mesh performance in various oils, such as n-hexane, mineral oil, olive oil, and diesel, the oil rejection rate was above 98%. The results show that the NaA zeolite-coated membrane is suitable for oil/water mixtures separation.

Declaration of Competing Interest

The authors declare that they have no known competing financial interests or personal relationships that could have appeared to influence the work reported in this paper.

Acknowledgement

This work was supported by Oklahoma State University; the Technology and Business Development Program (TBDP) and the United States Geological Survey (G16AP00077). We also give special thanks to Pamela Reynolds editing the manuscript.

Appendix A. Supplementary material

Download all supplementary files Help

The following are the Supplementary data to this article:

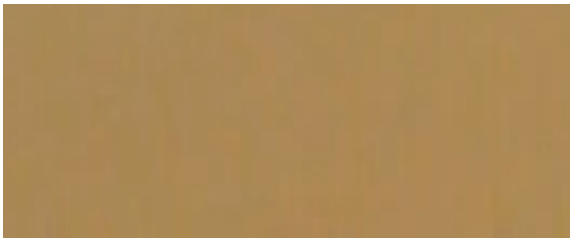

0:00 / 0:25

Download : **Download video (4MB)**

Supplementary video 1.

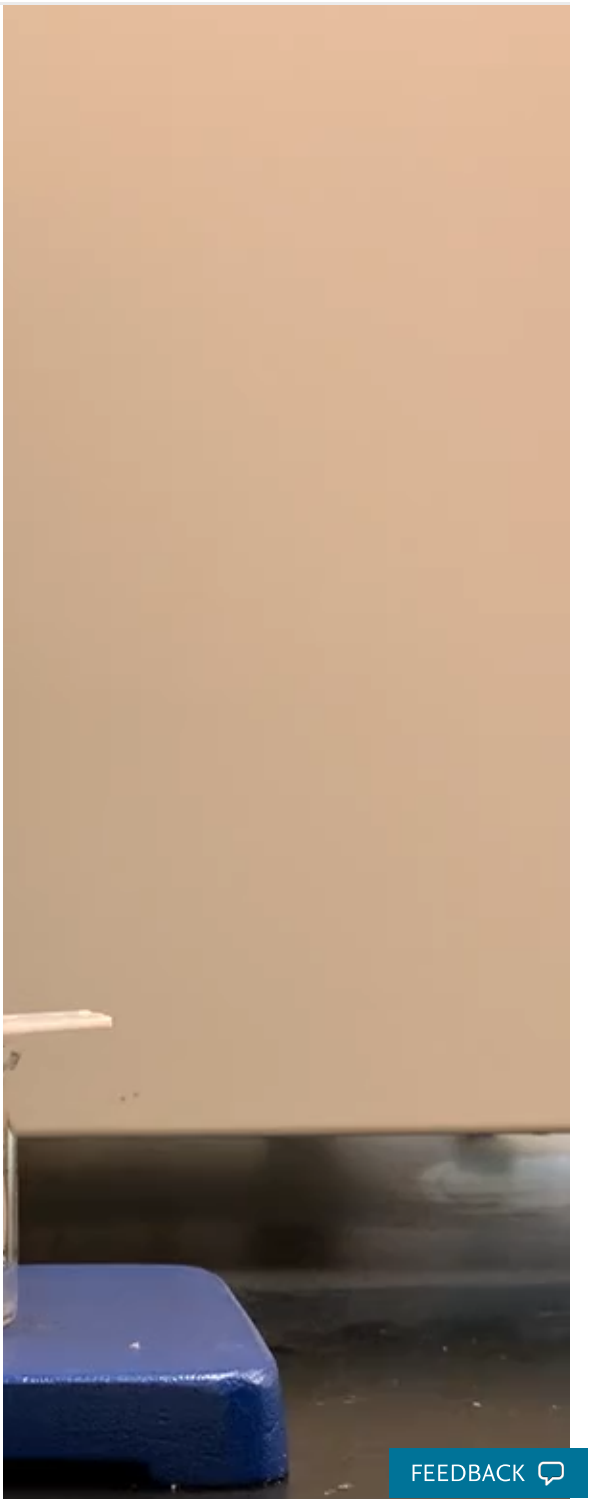

0:00 / 0:22

Download : **Download video (2MB)**

Supplementary video 2.

Download : **Download Word document (2MB)**

Supplementary data 3.

Recommended articles Citing articles (7)

References

[1] H. Liu, B. Geng, Y. Chen, H. Wang
Review on the aerogel-type oil sorbents derived from nanocellulose
Acs. Sustain. Chem. Eng., 5 (2016), pp. 49-66
View Record in Scopus Google Scholar

[2] Y. Liu, Z. Jing, T. Zhang, Q. Chen, F. Qiu, Y. Peng, S. Tang
Fabrication of functional biomass carbon aerogels derived from sisal fibers for application in selenium extraction
Food Bioprod. Process., 111 (2018), pp. 93-103
Article Download PDF View Record in Scopus Google Scholar

[3] Y. Liu, Y. Peng, T. Zhang, F. Qiu, D. Yuan

FEEDBACK

Superhydrophobic, ultralight and flexible biomass carbon aerogels derived from sisal fibers for highly efficient oil–water separation
Cellulose, 25 (2018), pp. 3067-3078
CrossRef View Record in Scopus Google Scholar

[4] F. Aguilera, J. Méndez, E. Pásaro, B. Laffon
Review on the effects of exposure to spilled oils on human health
J. Appl. Toxicol.: An Int. J., 30 (2010), pp. 291-301
View Record in Scopus Google Scholar

[5] R. Khurshid, M. Sheikh, S. Iqbal, Health of people working/living in the vicinity of an oil-polluted beach near Karachi, Pakistan, 2008.
Google Scholar

[6] J. Rong, F. Qiu, T. Zhang, X. Zhang, Y. Zhu, J. Xu, D. Yang, Y. Dai
A facile strategy toward 3D hydrophobic composite resin network decorated with biological ellipsoidal structure rapeseed flower carbon for enhanced oils and organic solvents selective absorption
Chem. Eng. J., 322 (2017), pp. 397-407
Article Download PDF View Record in Scopus Google Scholar

[7] D. Fragouli, A. Athanassiou
Oil spill recovery: graphene heaters absorb faster
Nat. Nanotechnol., 12 (2017), p. 406
CrossRef View Record in Scopus Google Scholar

[8] S.S. Banerjee, M.V. Joshi, R.V. Jayaram
Treatment of oil spill by sorption technique using fatty acid grafted sawdust
Chemosphere, 64 (2006), pp. 1026-1031
Article Download PDF View Record in Scopus Google Scholar

[9] T. Zhang, L. Kong, Y. Dai, X. Yue, J. Rong, F. Qiu, J. Pan
Enhanced oils and organic solvents absorption by polyurethane foams composites modified with MnO2 nanowires
Chem. Eng. J., 309 (2017), pp. 7-14
Article Download PDF View Record in Scopus Google Scholar

[10] C. Zhang, D. Yang, T. Zhang, F. Qiu, Y. Dai, J. Xu, Z. Jing
Synthesis of MnO2/poly (n-butylacrylate-co-butyl methacrylate-co-methyl methacrylate) hybrid resins for efficient oils and organic solvents absorption
J. Clean. Prod., 148 (2017), pp. 398-406
Article Download PDF View Record in Scopus Google Scholar

[11] T. Zhang, F. Hu, C. Zhang, D. Yang, F. Qiu, X. Peng
A novel multi-wall carbon nanotubes/poly (n-butylacrylate-co-butyl methacrylate) hybrid resin: synthesis and oil/organic solvents absorption
Fibers Polym., 18 (2017), pp. 1865-1873
CrossRef View Record in Scopus Google Scholar

[12] Z. Li, T. Zhang, F. Qiu, X. Yue, D. Yang, P. Li, Y. Zhu
Facile one-step fabrication of highly hydrophobic, renewable and mechanically flexible sponge with dynamic coating for efficient oil/water separation
J. Tai. Instit. Chem. Eng., 95 (2019), pp. 515-524
Article Download PDF View Record in Scopus Google Scholar

[13] J.-J. Li, L.-T. Zhu, Z.-H. Luo
Electrospun fibrous membrane with enhanced swithchable oil/water wettability for oily water separation

Chem. Eng. J., 287 (2016), pp. 474-481
Article Download PDF View Record in Scopus Google Scholar

[14] X. Zheng, Z. Guo, D. Tian, X. Zhang, W. Li, L. Jiang
Underwater self-cleaning scaly fabric membrane for oily water separation
ACS Appl. Mater. Interfaces, 7 (2015), pp. 4336-4343
CrossRef View Record in Scopus Google Scholar

[15] X. Yue, Z. Li, T. Zhang, D. Yang, F. Qiu
Design and fabrication of superwetting fiber-based membranes for oil/water separation applications
Chem. Eng. J. (2019)
Google Scholar

[16] Z. Pan, S. Cao, J. Li, Z. Du, F. Cheng
Anti-fouling TiO2 nanowires membrane for oil/water separation: synergetic effects of wettability and pore size
J. Membr. Sci., 572 (2019), pp. 596-606
Article Download PDF View Record in Scopus Google Scholar

[17] Z. Xiong, H. Lin, Y. Zhong, Y. Qin, T. Li, F. Liu
Robust superhydrophilic polylactide (PLA) membranes with a TiO 2 nano-particle inlaid surface for oil/water separation
J. Mater. Chem. A, 5 (2017), pp. 6538-6545
CrossRef View Record in Scopus Google Scholar

[18] Z.-X. Wang, C.-H. Lau, N.-Q. Zhang, Y.-P. Bai, L. Shao
Mussel-inspired tailoring of membrane wettability for harsh water treatment
J. Mater. Chem. A, 3 (2015), pp. 2650-2657
CrossRef View Record in Scopus Google Scholar

[19] T. Nguyen, F. Roddick, L. Fan
Biofouling of water treatment membranes: a review of the underlying causes, monitoring techniques and control measures
Membrane, 2 (2012), pp. 804-840
CrossRef View Record in Scopus Google Scholar

[20] P. Goh, A. Ismail
A review on inorganic membranes for desalination and wastewater treatment
Desalination, 434 (2018), pp. 60-80
Article Download PDF View Record in Scopus Google Scholar

[21] M. Elma, D.K. Wang, C. Yacou, J. Motuzas, J.C.D. da Costa
High performance interlayer-free mesoporous cobalt oxide silica membranes for desalination applications
Desalination, 365 (2015), pp. 308-315
Article Download PDF View Record in Scopus Google Scholar

[22] P. Swenson, B. Tanchuk, A. Gupta, W. An, S.M. Kuznicki
Pervaporative desalination of water using natural zeolite membranes
Desalination, 285 (2012), pp. 68-72
Article Download PDF View Record in Scopus Google Scholar

[23] R. Liu, S. Dangwal, I. Shaik, C. Aichele, S.-J. Kim
Hydrophilicity-controlled MFI-type zeolite-coated mesh for oil/water separation
Sep. Purif. Technol., 195 (2018), pp. 163-169
Article Download PDF View Record in Scopus Google Scholar

[24] C.-j. Liu, U. Burghaus, F. Besenbacher, Z.L. Wang, Preparation and characterization of nanomaterials for sustainable energy production, in, ACS Publications, 2010.

Google Scholar

[25] R. Ameloot, F. Vermoortele, W. Vanhove, M.B. Roeffaers, B.F. Sels, D.E. De Vos
Interfacial synthesis of hollow metal–organic framework capsules demonstrating selective permeability
Nat. Chem., 3 (2011), p. 382
CrossRef View Record in Scopus Google Scholar

[26] R. Das, M.E. Ali, S.B.A. Hamid, S. Ramakrishna, Z.Z. Chowdhury
Carbon nanotube membranes for water purification: a bright future in water desalination
Desalination, 336 (2014), pp. 97-109
Article Download PDF View Record in Scopus Google Scholar

[27] P. Goh, A. Ismail
Graphene-based nanomaterial: the state-of-the-art material for cutting edge desalination technology
Desalination, 356 (2015), pp. 115-128
Article Download PDF View Record in Scopus Google Scholar

[28] C. Li, A.L. Ward, S.E. Doris, T.A. Pascal, D. Prendergast, B. Helms
Polysulfide-blocking microporous polymer membrane tailored for hybrid Li-sulfur flow batteries
Nano Lett., 15 (2015), pp. 5724-5729
CrossRef View Record in Scopus Google Scholar

[29] G.A. Elia, J. Hassoun
A gel polymer membrane for lithium-ion oxygen battery
Solid State Ion., 287 (2016), pp. 22-27
Article Download PDF View Record in Scopus Google Scholar

[30] T. Hajilounezhad, D.M. Ajiboye, M.R. Maschmann
Evaluating the forces generated during carbon nanotube forest growth and self-assembly
Materialia, 100371 (2019)
Google Scholar

[31] M. Servatan, M. Ghadiri, A.T. Damanabi, F. Bahadori, P. Zarrintaj, Z. Ahmadi, H. Vahabi, M.R. Saeb
Zeolite-based catalysts for exergy efficiency enhancement: the insights gained from nanotechnology
Mater. Today., 5 (2018), pp. 15868-15876
Article Download PDF View Record in Scopus Google Scholar

[32] X. Feng, Z. Zong, S.K. Elsaidi, J.B. Jasinski, R. Krishna, P.K. Thallapally, M. Carreon
Kr/Xe separation over a chabazite zeolite membrane
J. Am. Chem. Soc., 138 (2016), pp. 9791-9794
CrossRef View Record in Scopus Google Scholar

[33] C. Baerlocher, L.B. McCusker, D.H. Olson
Atlas of Zeolite Framework Types
Elsevier (2007)
Google Scholar

[34] X.-L. Wei, S. Liang, Y.-Y. Xu, Y.-L. Sun, J.-F. An, Z.-S. Chao
Patching NaA zeolite membrane by adding methylcellulose into the synthesis gel
J. Membr. Sci., 530 (2017), pp. 240-249
Article Download PDF View Record in Scopus Google Scholar

[35] S.M. Lee, Y.H. Lee, J.R. Grace, A. Li, C.J. Lim, F. Fotovat, A. Schaadt, R.J. White, S.S. Kim
Gas permeation properties of NaA zeolite membranes: effect of silica source on hydrogel synthesis and layer thickness
J. Porous Mater., 1–9 (2019)
Google Scholar

[36] A.D.K.e. al., Fabrication, characterization, and application of palladium composite membrane on porous stainless steel substrate with Nay zeolite as an intermediate layer for hydrogen purification, Int. J. Hydrogen Energy, 44 (2019) 2889–2904.
Google Scholar

[37] J. Jiang, L. Peng, X. Wang, H. Qiu, M. Ji, X. Gu
Effect of Si/Al ratio in the framework on the pervaporation properties of hollow fiber CHA zeolite membranes
Micropor. Mesopor. Mater., 273 (2019), pp. 196-202
Article Download PDF View Record in Scopus Google Scholar

[38] X.-Q. Li, P.-Y. Zheng, J.-K. Wu, N.-X. Wang, S.-L. Ji, Z.-H. Yu, Q.-F. An
Facial build-up of acid-resistance skin for high-stability zeolite NaA membrane
J. Membr. Sci., 573 (2019), pp. 55-63
Article Download PDF CrossRef View Record in Scopus Google Scholar

[39] Y. Liu, Z. Yang, C. Yu, X. Gu, N. Xu
Effect of seeding methods on growth of NaA zeolite membranes
Micropor. Mesopor. Mater., 143 (2011), pp. 348-356
Article Download PDF View Record in Scopus Google Scholar

[40] H. Ju, B.D. McCloskey, A.C. Sagle, Y.-H. Wu, V.A. Kusuma, B.D. Freeman
Crosslinked poly (ethylene oxide) fouling resistant coating materials for oil/water separation
J. Membr. Sci., 307 (2008), pp. 260-267
Article Download PDF CrossRef View Record in Scopus Google Scholar

[41] H.-J. Li, Y.-M. Cao, J.-J. Qin, X.-M. Jie, T.-H. Wang, J.-H. Liu, Q. Yuan
Development and characterization of anti-fouling cellulose hollow fiber UF membranes for oil–water separation
J. Membr. Sci., 279 (2006), pp. 328-335
Article Download PDF View Record in Scopus Google Scholar

[42] S. Kasemset, A. Lee, D.J. Miller, B.D. Freeman, M.M. Sharma
Effect of polydopamine deposition conditions on fouling resistance, physical properties, and permeation properties of reverse osmosis membranes in oil/water separation
J. Membr. Sci., 425 (2013), pp. 208-216
Article Download PDF View Record in Scopus Google Scholar

[43] S. Zhang, F. Lu, L. Tao, N. Liu, C. Gao, L. Feng, Y. Wei
Bio-inspired anti-oil-fouling chitosan-coated mesh for oil/water separation suitable for broad pH range and hyper-saline environments
ACS Appl. Mater. Interfaces., 5 (2013), pp. 11971-11976
CrossRef View Record in Scopus Google Scholar

[44] Z. Wang, S. Lin
Membrane fouling and wetting in membrane distillation and their mitigation by novel membranes with special wettability
Water Res., 112 (2017), pp. 38-47
Article Download PDF CrossRef View Record in Scopus Google Scholar

[45] L. Feng, Z. Zhang, Z. Mai, Y. Ma, B. Liu, L. Jiang, D. Zhu
A super-hydrophobic and super-oleophilic coating mesh film for the separation of oil and water
Angew. Chem. Int. Ed., 43 (2004), pp. 2012-2014
CrossRef View Record in Scopus Google Scholar

[46] Z. Xue, S. Wang, L. Lin, L. Chen, M. Liu, L. Feng, L. Jiang
A novel superhydrophilic and underwater superoleophobic hydrogel-coated mesh for oil/water separation

Adv. Mater., 23 (2011), pp. 4270-4273
CrossRef View Record in Scopus Google Scholar

[47] D. Tian, X. Zhang, Y. Tian, Y. Wu, X. Wang, J. Zhai, L. Jiang
Photo-induced water–oil separation based on switchable superhydrophobicity–superhydrophilicity and underwater superoleophobicity of the aligned ZnO nanorod array-coated mesh films
J. Mater. Chem., 22 (2012), pp. 19652-19657
CrossRef View Record in Scopus Google Scholar

[48] D. Tian, X. Zhang, X. Wang, J. Zhai, L. Jiang
Micro/nanoscale hierarchical structured ZnO mesh film for separation of water and oil
Phys. Chem. Chem. Phys., 13 (2011), pp. 14606-14610
CrossRef View Record in Scopus Google Scholar

[49] L. Yan, J. Li, W. Li, F. Zha, H. Feng, D. Hu
A photo-induced ZnO coated mesh for on-demand oil/water separation based on switchable wettability
Mater. Lett., 163 (2016), pp. 247-249
Article Download PDF View Record in Scopus Google Scholar

[50] J. Li, L. Yan, W. Hu, D. Li, F. Zha, Z. Lei
Facile fabrication of underwater superoleophobic TiO2 coated mesh for highly efficient oil/water separation
Colloids Surf A, 489 (2016), pp. 441-446
Article Download PDF View Record in Scopus Google Scholar

[51] J. Li, D. Li, W. Li, H. Li, H. She, F. Zha
Facile fabrication of underwater superoleophobic SiO2 coated meshes for separation of polluted oils from corrosive and hot water
Sep. Purif. Technol., 168 (2016), pp. 209-214
Article Download PDF View Record in Scopus Google Scholar

[52] M.K. Kang, R. Huang
Effect of surface tension on swell-induced surface instability of substrate-confined hydrogel layers
J. Soft. Matter., 6 (2010), pp. 5736-5742
CrossRef View Record in Scopus Google Scholar

[53] R. Liu, S. Young, S. Dangwal, I. Shaik, E. Echeverria, D. McIlroy, C. Aichele, S.-J. Kim
Boron substituted MFI-type zeolite-coated mesh for oil-water separation
Colloids Surf. A, 550 (2018), pp. 108-114
Article Download PDF View Record in Scopus Google Scholar

[54] J. Zhang, W. Liu
Thin porous metal sheet-supported NaA zeolite membrane for water/ethanol separation
J. Membr. Sci., 371 (2011), pp. 197-210
Article Download PDF CrossRef View Record in Scopus Google Scholar

[55] J. Li, D. Li, Y. Yang, J. Li, F. Zha, Z. Lei
A prewetting induced underwater superoleophobic or underoil (super) hydrophobic waste potato residue-coated mesh for selective efficient oil/water separation
Green. Chem., 18 (2016), pp. 541-549
CrossRef View Record in Scopus Google Scholar

[56] A. Loiola, J. Andrade, J. Sasaki, L. Da Silva
Structural analysis of zeolite NaA synthesized by a cost-effective hydrothermal method using kaolin and its use as water softener
J. Colloid Interface Sci., 367 (2012), pp. 34-39

Article Download PDF View Record in Scopus Google Scholar

[57] J. Liu, Q. Yin, H. Zhang, Y. Yan, Z. Yi
Continuous removal of Cr (VI) and Orange II over a novel Fe0-NaA zeolite membrane catalyst
Sep. Purif. Technol., 209 (2019), pp. 734-740
Article Download PDF View Record in Scopus Google Scholar

[58] Q. Wen, J. Di, L. Jiang, J. Yu, R. Xu
Zeolite-coated mesh film for efficient oil–water separation
Chem. Sci., 4 (2013), pp. 591-595
View Record in Scopus Google Scholar

[59] A.K. Kota, G. Kwon, W. Choi, J.M. Mabry, A. Tuteja
Hygro-responsive membranes for effective oil–water separation
Nat. Commun., 3 (2012), p. 1025
View Record in Scopus Google Scholar

[60] A. Huang, L.-H. Chen, C.-C. Kan, T.-Y. Hsu, S.-E. Wu, K.K. Jana, K.-L. Tung
Fabrication of zinc oxide nanostructure coated membranes for efficient oil/water separation
J. Membr. Sci., 566 (2018), pp. 249-257
Article Download PDF View Record in Scopus Google Scholar

[61] M. Guisnet, Q. Wang, G. Giannetto
Dealumination of NH 4 NaY zeolites through hydrothermal treatment: kinetic order with respect to aluminium
Catal. Lett., 4 (1990), pp. 299-302
View Record in Scopus Google Scholar

View Abstract